

Building an interferometer at the edge of space: pointing and phase control system for BETTII

Maxime J. Rizzo^{a,b}, S. A. Rinehart^b, J. B. Alcorn^c, R. B. Barclay^b, R. K. Barry^b,
D. J. Benford^b, A. Dhabal^{a,b}, D. J. Fixsen^a, A. S. Gore^d, S. Johnson-Shapoval^a,
D. T. Leisawitz^b, S. F. Maher^b, L. G. Mundy^a, A. Papageorgiou^e, E. Pascale^e, A. Rau^f,
R. F. Silverberg^b, P. Taraschi^g, T. J. Veach^b, S. Weinreich^h

^aUniversity of Maryland, College Park, MD 20741, USA

^bNASA Goddard Space Flight Center, Greenbelt, MD 20770, USA

^cUniversity of Alabama, Huntsville, AL, USA

^dUniversity of Illinois at Urbana-Champaign, Champaign, IL, USA

^eCardiff University, Cardiff, UK

^fNaperville North High School, Naperville, IL, USA

^gAlfred University, Alfred, NY, USA

^hBrown University, Providence, RI, USA

ABSTRACT

We propose an architecture for the control system of BETTII,¹ a far-infrared, balloon-borne interferometer with a baseline of 8 meters. This system involves multiple synchronized control loops for real-time pointing control and precise attitude knowledge. This will enable accurate phase estimation and control, a necessity for successful interferometry. We present the overall control strategy and describe our flight hardware in detail. We also show our current test setup and the first results of our coarse pointing loop.

Keywords: Interferometer, control system, pointing, balloon, Fourier transform spectrometer, spatio-spectral interferometry

1. INTRODUCTION

The Balloon Experimental Twin Telescope for Infrared Interferometry (BETTII) is an instrument aimed at studying the far-infrared universe at high angular resolution. With its 8-meter baseline, it will provide sub-arcsecond angular resolutions in the 30 – 90 μm range, as well as low spectral resolution for all the sources in a 2x2 arcmin field of view. This technique, that requires both spatial and spectral Fourier reconstruction of the astronomical scene, is called "double-Fourier" interferometry.² It has been successfully implemented at multiple occasions,^{3,4} and is a potential technique for future space-based, far-IR missions.⁵⁻⁷

BETTII will use this technique on a platform flying above most of the atmosphere, in order to get access to the far-IR universe which is blocked from the ground. Despite being at the edge of space, there is still a large amount of background noise that limits the sensitivity of the instrument. In addition to the pure thermal noise, it is very important for the interferometric phase to be well understood and well-behaved during the flight, in order to ensure the integrity of the scientific data which is encoded in both axes of interferogram scans. This explains the need for a robust control system to ensure that the payload is stable during observing phases, and that the attitude is known precisely at all times.

Two other papers in these proceedings discuss the general BETTII project status (Rinehart et al., 2014), and the optical system (Veach et al. 2014). We present here the control architecture of the mission. In section 2, we discuss the pointing and phase requirements and give an overview of our architecture and strategy. In section 3, we present details of the important components in the control system. Finally, in section 4, we show our current pointing test setup and discuss some preliminary results obtained with flight hardware, along with our plan to test the full control system.

Author contact: M. J. Rizzo, mrizzo@astro.umd.edu

2. CONTROL SYSTEM OVERVIEW

2.1 Pointing and phase requirements

The 3D rendering in Fig. 1 shows a realistic overview of the system. A schematic diagram of BETTII is also shown in Fig. 2. To form the interferometric signal, the two separate optical paths need to be combined at the beamsplitter, inside the central cryostat. The goal of the control system is two-fold. The first goal is to make sure that the beams coming from the two arms are overlapping at the detectors, in order to create interferometric fringes. The second goal is to make sure they combine while having a controlled and known phase. Indeed, the scientific signal is obtained by recording the intensity of the image from the combined beams on the detectors, as we vary the phase between them back and forth around the point of zero phase difference. This is the same process that is used in a traditional Fourier transform spectrometer.⁸

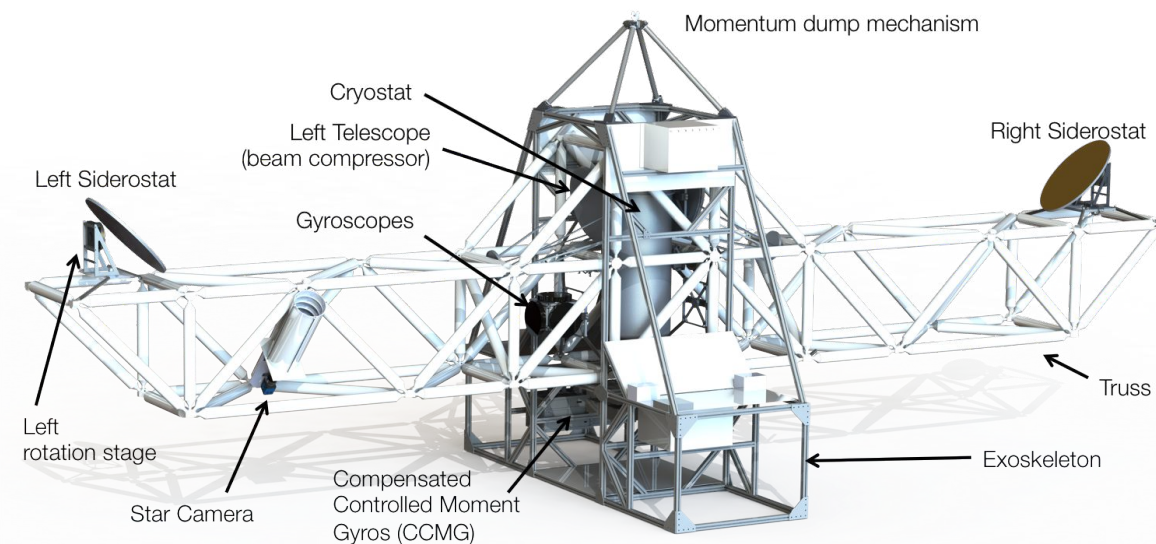


Figure 1. BETTII realistic render. The distance between the center of both siderostats is 8 meters. BETTII's optical train is attached to a carbon fiber truss, while the electronics, batteries, and the azimuth actuator are attached onto an aluminum exoskeleton. The truss is attached to the exoskeleton through passive vibration dampers.

With 50 cm collecting mirrors (the "siderostats"), our beam size is about 40" and our pixel size is 13" at the shorter science wavelengths. A good beam overlap will be achieved if the combination occurs within $\sim 10\%$ of a detector pixel. Hence we set our differential pointing requirement to 1.5". As we discuss in the next section, this requires the use of a near-IR tracking channel which shares most of the optical path with the science instrument. However, in order to use this tracking channel on a guide star with reasonable accuracy, the star needs to be within 15" of the field center. This sets our overall required pointing stability during flight.

If the phase between the two beams is stable, then we can modulate it by using a linear mechanism, the Cold Delay Line (see section 3.6). However, the phase can vary due to asymmetries between the two arms of the interferometer, or due to pointing errors. With our baseline of 8 m, a mispointing of the main truss by 1" corresponds to $40 \mu\text{m}$ of optical path difference (OPD), which is significant considering our wavelength range of $30 - 90 \mu\text{m}$. We have carefully derived analytic expressions to describe the impact of phase uncertainties on the scientific signal-to-noise ratio (Rizzo et al. 2014, PASP, submitted). To optimize our sensitivity, we determine that a post-flight attitude knowledge of 0.1" rms is necessary over periods of 1.5 minutes. However, it is not necessary for us to *control* the payload to this level. Interferometry cares about phase - and an error in pointing of the interferometer can be corrected directly in the phase domain as long as the beams are combined properly.

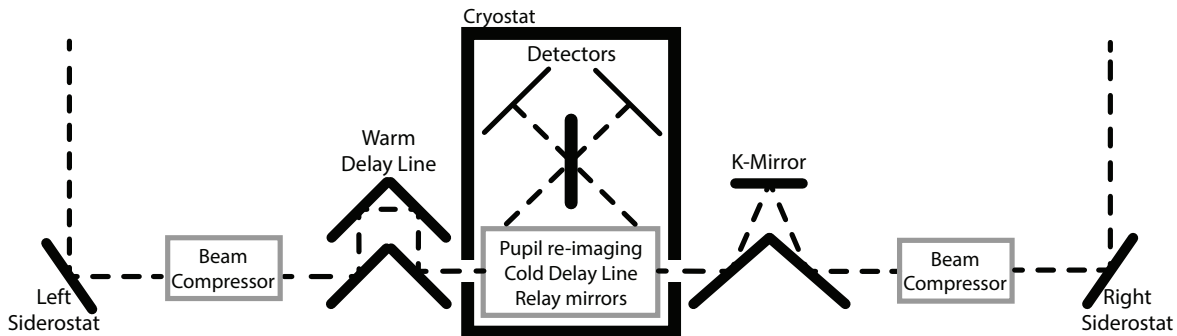


Figure 2. Optical schematic for BETTII, with more details than what is shown in Fig 1. This is not to scale. The cryostat optics layout is simplified, see Veach et al. (2014, these proceedings) for more details. The optics that are sketched or mentioned in the cryostat are the far-IR optics and are all at 4 K. For clarity, we do not show the LN₂ compartment, which contains BETTII's angle sensor.

During flight, it is necessary to keep the phase within the range of the Cold Delay Line (we set a requirement of $< 100 \mu\text{m}$), and stable enough so that it is not changing fast with respect to a single fringe packet (we set the requirement to $< 5 \mu\text{m}$ over 200 ms to keep Nyquist sampling of the fringes). Finally, the phase needs to be stable during a single integration of 2.5 ms to avoid smearing (see Section 2.4). We set this last stability requirement to $< 1 \mu\text{m}$. Without the ability to *freeze* the fringes down to these levels for each relevant timescale, a large amount of signal is lost due to decreased visibility of the interferogram.

2.2 Overall control strategy

The payload is controlled in an altitude/azimuth fashion. The relevant coordinate system is centered on a near-IR guide star, one axis being the boresight of the telescope, a second axis being the elevation direction, and the third axis being defined to form an orthogonal reference frame. We call the third axis "cross-elevation". In this coordinate frame, only cross-elevation mispointings contribute to phase errors, since mispointings in the elevation direction are orthogonal to the baseline vector and have no impact on the phase. All science targets need to have a guide star in their vicinity.

The control is done at three levels. The top level is a coarse control loop that maintains the payload pointed within 15" of the guide star at all times. In flight, the system is excited by pendulum modes that can have large amplitudes and frequencies that can be up to 0.5 Hz.⁹ This loop uses low-bandwidth actuators that are described in sections 3.1 and 3.2. A block diagram showing the coarse control loop is shown in Fig. 3.

The second level is a more accurate level of pointing correction. Instead of correcting the attitude of the whole payload, this loop controls fast steering tip/tilt mirrors that are placed at the pupil of each arm. The "Angle Sensor", a near-IR H1RG detector in the nitrogen-cooled compartment of the cryostat (not shown in Fig. 2), images the guide star seen through each arm on separate readout windows, and keeps the two images on preset locations that maximize overlap in the science channels. While the corrections are made, an encoder reads out how much tip or tilt is being applied to the stages to keep the guide star at its position, and common-mode deviations from nominal tip/tilt angles are sent back to the top-level loop, to make sure that there is no drift in the overall pointing.

Finally, the third level is the phase control. A robust estimator, to be discussed extensively in a subsequent paper (Rizzo et al. 2014, in prep.), constantly monitors our attitude error, and converts it into a phase error. This error signal is fed into another delay line (the Warm Delay Line or WDL, see Section 3.5), located in one arm of the interferometer). This delay line is a linear stage and will compensate for this phase error by increasing or shortening the optical pathlength in one arm only, so that the differential phase at the entrance of the cryogenic instrument is controlled to a minimum. To correct for drifts, a phase reference needs to be determined frequently by finding fringes on a point source in the science channel. While it is critical to know the estimated phase to high accuracy and at all times, the requirements on the actual controls of the phase are less

stringent, as we can always reconstruct the phase axis of the interferogram after the flight if there is sufficient stability and knowledge.

While all these control loops are interacting, an independent control loop is always scanning the CDL over a fixed stroke and with a constant velocity profile. If the rest of the control system does its job and produces good overlap and decent control of the phase entering the cryostat, the CDL scan will provide the lag-spectra used to recover the scientific information in the astronomical scene.

2.3 Control modes and transitions

BETTII features two main control modes: a slew mode, and a tracking mode. There are also two transition modes: a Lost-In-Space (LIS) mode, and an Acquire mode. Each of these four modes has a different set of PID parameters associated to them.

The LIS mode allows us to recover our attitude when we lose knowledge of it. Once the attitude is determined, we switch to Slew Mode where the payload is rotated in Azimuth and the siderostats are rotated in Elevation, to point at our desired target. The switch of the modes is triggered by the flight computer. During the LIS and the Slew mode, only the top-level coarse pointing loop is active.

Once we arrive close to the target, we transition to Acquire mode. This mode is challenging because its testing is difficult from the ground. In this mode, we look for the guide star in the near-IR Angle Sensor windows. First, we take full-frame pictures to optimize our chances to find the star. We then progressively reduce the frame size while increasing the frame rate, in order to close in on the guide star and get it on our desired location in each window. The error between the current star position and its desired location is fed to the tip/tilt stages and the coarse pointing loop. This desired location, which corresponds to an overlap of the science beams, needs to be determined through a calibration procedure during the first phases of the flight.

This exercise might require real-time tuning of the PID gains of all control loops. Once the Angle Sensor has reached full speed (400 Hz) and the guide star is kept stable at its desired location, science observations are now possible. We switch to Tracking mode, although there is no significant change in the PID gains from the end of the Acquire mode.

2.4 Synchronization

Synchronization is a key element to our system. Having non synchronized devices and control loops can introduce unexpected beat frequencies that could be seen in the science detector bands, or introduce vibrations that would generate phase noise. By synchronizing the science detector readout and our interferogram scans with the rest of the control system, we guarantee that we do not see such artifacts. For example, should a vibration be created by one mechanism, if the mechanism is synchronized with the detector readout we will observe the effects of this vibration always at the same, known phase - a pattern that can be more easily taken out in post-processing.

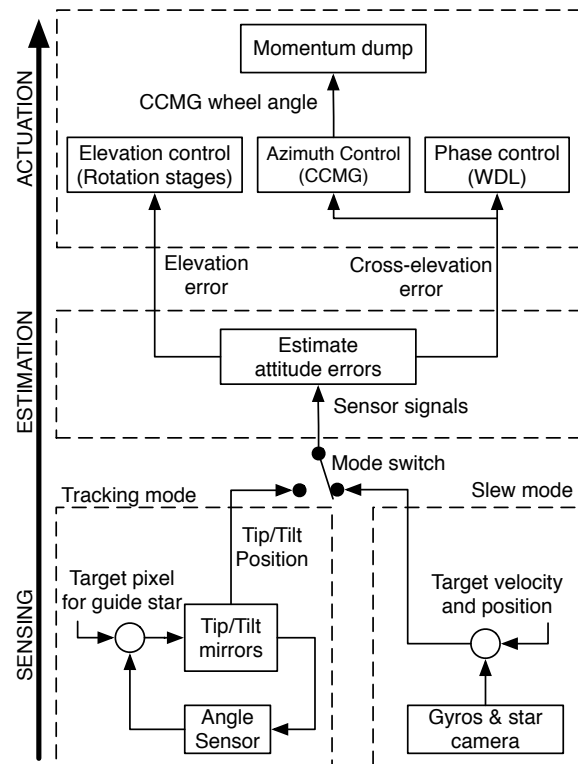


Figure 3. Overall control flow of the pointing system. This diagram shows the three steps that are taken at the heartbeat rate (400 Hz, see Section 2.4): 1) Sensing, 2) Estimation, and 3) Actuation. Two modes of operations are shown, the slew mode and the tracking mode. The switch between the sensors occurs before going into the estimator.

Without synchronization, the phase at which we observe that vibration jitters, and could make it extremely hard to track in the data products.¹⁰

As a result, we favor hardware that has the capability of being synchronized with an external clock, and try to use as many analog devices as possible. We have mostly succeeded in this endeavor and we are confident that our choice of mechanisms and synchronization scheme will greatly reduce the time of data reduction.

We choose a National Instrument cRIO (see Section 3.9), which can generate our master clock signal at 50 MHz. The other clocks are derived from this master clock in a cascade of integer dividers, as shown in Fig 4. Some dividers are imposed by the architecture of the science detector readout electronics.

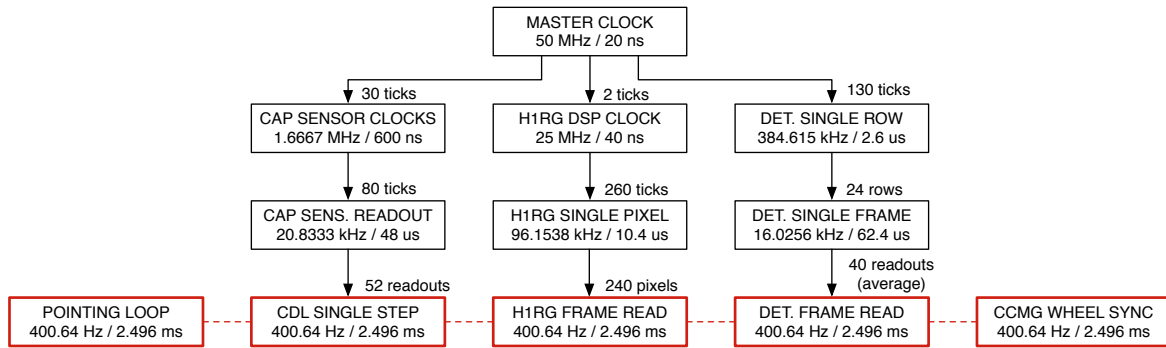


Figure 4. The BETTII master clock and its dividers, driven by the cap sensor clock requirements, the H1RG readout electronics, and the science detector readout electronics. The main heart beat for the entire system is at ~ 400.64 Hz, or exactly 124800 master clock ticks. The capacitive sensors are used in the CDL and the WDL.

All pointing and phase processes on BETTII happen at a heart beat of ~ 400 Hz. In particular, the main pointing control loop (Fig. 3) is operated at that frequency.

3. CONTROL SYSTEM HARDWARE

3.1 Azimuth control

Instead of using a traditional system of inertia wheels, BETTII uses two counter-rotating wheels that constantly spin at ~ 3004 rpm (one revolution in exactly 998400 master clock ticks). The device is called "CCMG", for Compensated Controlled Moment Gyros (Fig. 5(a)). The two wheels are connected to shafts that share the same gear box, and can provide a total momentum of 10.8 Nms. A stepper motor is used to turn the wheels shafts simultaneously. A change in the wheels' angle provides a torque.

The high speed of the wheels allows for a vibration signature that does not change with time, hence allowing for effective mitigation. In addition, it reduces the power usage; both these advantages led us to choose this design over a single-wheel configuration.

The two wheels are controlled through a DMC 4020 from Galil Motion. They are synchronized exactly eight times per revolution to one another, in order to keep the phase between them constant on average and to lock the potential beat frequency between them.

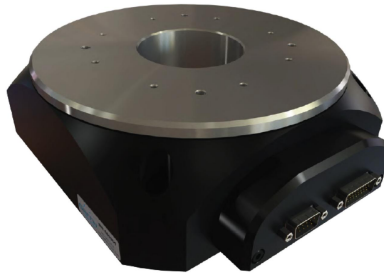
The CCMG was tested at flight temperature and pressures and proved to operate well. We routinely use the device today in our control tests.

3.2 Elevation control

The two flat mirrors at the end of the BETTII truss are rotated about the optical axis to provide elevation control. Our rotation stages are from Griffin Motion (serial RTS-DD-200-S-0-S-S-A-02, see Fig. 5(b)). In order to accommodate our requirements, we helped the company upgrade their original family of rotation stages by adding two major features. First, they now use a new RENISHAW encoder (RESOLUTE ETR), that provides absolute position knowledge to 0.19" over the full temperature range of our application. Second, for smoothness



(a) CCMG



(b) Griffin rotation stage



(c) Fiber optic gyroscope

Figure 5. Main hardware for the coarse pointing control loop.

of motion at velocities comparable to the Earth's rate, they now use a AISI 52100 steel race with ceramic balls, prepared with Braycote 815Z oil.

The performance of the original stages was marginal for our application, and we observed problematic friction and stick-slip behavior at low temperatures, which was making it hard to follow inertial targets across the sky. We attributed the problem to the bearing and the former encoder step size of $0.9''$, which sparked the discussion with the company. Despite the difficulty, low-speed tracking accuracy on the order of $\sim 15''$ rms was achieved. We expect to be able to do much better with the new generation.

The stages are controlled through integrated motion controllers (DMC 4040 from Galil Motion, with linear drivers). They take commands from the cRIO and close the loop on their own, using the stage's encoder. All rotation stages are synchronized on one single controller.

3.3 Gyroscopes

We use three fiber optics gyroscopes (Optolink SRS-2000, see Fig. 5(c)), mounted at 90 degrees from each other. These gyroscopes are rated to -40 C. We have completed extensive tests of these devices and they agree to the manufacturer's specifications very well. They have a bandwidth of 50 Hz, and the rms velocity variance integrated over the full bandwidth is ~ 0.2 arcsec/s rms. This number can be reduced to ~ 0.1 arcsec/s rms, but then the spectrum exhibits higher noise levels at some very specific frequencies, which we attribute to a signature of the internal gyroscope phase control loop. A random phase error can be introduced that smoothens the spectrum of the signal, while raising the overall noise level to 0.2 arcsec/s, rms.

The gyroscope keeps its performance when it is used in a balloon environment. When cold, the device uses three times more power, since it activates a Peltier cooler that controls the temperature of the light source inside the device (22 ± 0.5 degrees C).

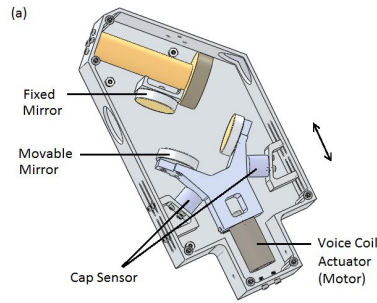
3.4 Tip/tilt mirrors

Our fast-steering tip/tilt mechanisms are modified S330.8SL stages from Physik Instrumente (Fig. 6(a)). They have a range of ± 7.5 mrad and a resolution of $0.2 \mu\text{rad}$. Their encoder's design has been modified to accommodate a wider temperature range, and they have been rated down to -40 C and low pressures. The stages can be operated both in open and closed-loop with E-616 electronics from the same company, that take DC voltage inputs. The electronics have not been rated down to low pressures and are a point of concern since they carry a lot of electrolytic capacitors, that could be a point of failure. We will do more testing on these electronics, but we are confident that they will not be a problem during flight. These electronics have been flown on a sounding rocket before,¹¹ and used a potting compound that made them operate well at low pressure and temperatures.

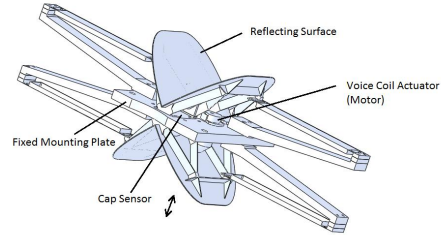
The electronics are controlled with analog signals, and the sensors are read out with analog signals too. However, they contain a system that converts 10 VDC to 100 VDC, which contains an oscillator and could possibly radiate in our science bands. Fortunately, the oscillator can and will be synchronized with a 200 kHz clock derived from our master clock.



(a) Tip Tilt mirrors of various sizes (www.pi.ws)



(b) Warm Delay Line CAD model



(c) Cold Delay line CAD model

Figure 6. Tip Tilt and phase loop hardware.

The tip/tilt platform is Invar, so it is best matched to a Zerodur mirror in terms of CTE. These are the only mirrors on BETTII which are not made out of aluminum. The mirrors are commercially available, 5 cm in diameter and 14 mm thick. They are bonded onto the platform with a slow-drying, two-component epoxy, 3M Scotchweld No. 2216.

Preliminary tests of the stages with the mirror load show no noticeable difference in bandwidth from the unloaded stages. The measured bandwidth is very close from the specified values (~ 130 Hz open-loop at 10% of full amplitude), and does not seem to be affected noticeably by the mirror's inertia.

3.5 Warm delay line

The warm delay line (WDL, see Fig. 6(b)) corrects for external OPD between the two arms of the interferometer caused by mispointings and other phase noise sources. The delay line consists of 4 mirrors arranged at 45 degrees to the incoming beam, two of which are fixed and two are movable. The adjustable mirrors are connected to a support mounted on a low friction stage that can be moved back and forth using a voice coil actuator. The support has 2 flat areas which are used as the target of 2 capacitive sensors to read the distance. The sensor (Microsense Model 8800 with 2811 probe) and the target surface on the stage are both oriented at an angle of 66.4 degrees to the direction of motion to ensure that the 4 mm sensor range corresponds to a 10 mm movement range of the stage. This movement range of the stage allows for a maximum range of 20 mm for the OPD. The variable delay length is controlled by a feedback control loop between the sensors and actuator. After tuning the control loop gains, the system was tested for various sinusoidal inputs that represent the expected pendulum modes. Although the delay errors cannot be controlled to sub- μm levels, they can be known down to $\sim 0.3 \mu\text{m}$.

Errors in control of the WDL within three different timescales have been achieved. At all times, the WDL error is less than $70 \mu\text{m}$, which is sufficient for ensuring that the fringe pattern for all sources within the FOV falls within the CDL scan range. In the timescale of 200 ms, which roughly corresponds to the scan period of a fringe packet by the CDL, the WDL rms error is $4.5 \mu\text{m}$, which is sufficient to ensure Nyquist sampling of the fringes. Also the WDL is stable to within $0.5 \mu\text{m}$ over a period of 2.5 ms, which ensures coherence over the science detector integration and read-out time.

3.6 Cold delay line

The cold delay line (CDL, see Fig. 6(c)) is used to sweep the zero path difference (ZPD) across the array field of view to cover the required sky field of view and spectral resolution. It has 4 mirrors rotated at 45 degrees to the two incoming beams coming from the two arms (see Figure 18). The four mirrors move as a single unit simultaneously decreasing the optical path on one of the beams and increase it on the other, thereby achieving a 4-fold OPD between the two interfering beams. A 2 mm stroke delay line produces the required OPD of 8 mm. The CDL uses two capacitive sensors (Microsense Model 4810 with 2821V probe) and two voice coil actuators, with a range of 2 mm. All are integrated into a single PID control loop. Unlike the WDL, the CDL operates at cryogenic temperatures (4.2 K in flight), so instead of a regular linear bearing, it uses cryogenic flexures.

3.7 Momentum dump

A momentum dump mechanism is used to unload the momentum that has been built up in the payload. It is a Phytron VSS42 with 200 steps per revolution. It is connected to a two-bearing system that very lightly couples the payload to the rotation of the balloon train. We control it with the same Galil DMC 4020 that also control the CCMG gimbal stepper motor.

3.8 Star camera

The star camera is made in-house to reduce costs. The camera is a PCO.Edge camera with a CameraLink readout card. This allows for low-noise, fast full-frame readout of the CMOS sensor. It is coupled to a Nikon Nikkor 300 mm lens used at $f/2.8$. The camera has a field of view of 3.18×2.68 degrees and can produce usable images with 100 ms exposures from the ground. A software developed for the EBEX mission¹² and modified for BETTII by Cardiff University processes the images and provides attitude knowledge within 1" rms in RA and Dec, and $\sim 40''$ in roll about the boresight. The software solves the Lost-In-Space problem with no a priori information about the location in about 2 s. This is based on routine observations from Greenbelt, MD, where seeing conditions are usually unfavorable, so we expect increased performance in flight.

The camera's cooling system is modified. We removed the fan and epoxied copper straps in the heat sink's fins, that we connect to a radiator. The camera operates fine in air at room temperature. Although the camera housing gets warm, the chip is kept at 5.5 C with a Peltier device.

3.9 Flight computers

The control system is orchestrated by a National Instrument cRIO (NI-9082 with extension chassis). All input/output is going through protocol-specific I/O modules. The cRIO generates and distributes the master 50 MHz clock. A block diagram of the system is shown in Fig. 7.

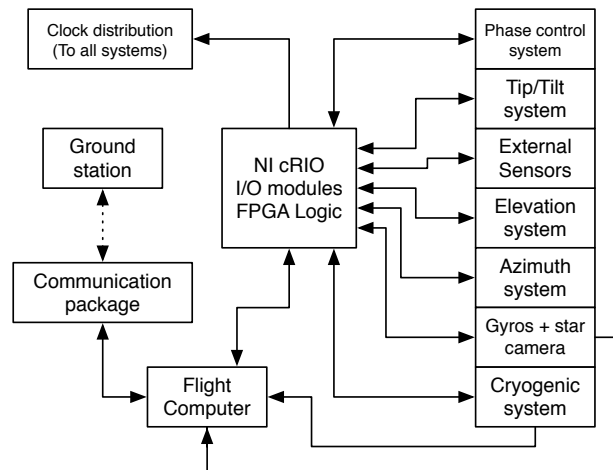


Figure 7. BETTII block diagram, showing the central role of the NI cRIO in the system. Each block represents a subsystem composed of a sensor/actuator and its electronics box and power distribution. The Cryogenic System, not mentioned in details in this paper, contains the science detectors, the HIRG angle sensor, and the thermometry management inside the cryostat. The External Sensors subsystem contains sensors that are not critical for the control loop, such as a magnetometer, inclinometers, accelerometers, etc.

The control code is written in Labview FPGA, which interfaces to the ground station through telemetry with a JAVA GUI code developed in-house. The GUI allows us to monitor real-time data and change the PID gains for all the system's control loops.

Another flight computer, which purpose is mainly to process the star camera and HIRG images, is used in addition to the cRIO. This computer must support multiple PCI Express slots (for the star camera and science

detector readout interface), ECC (Error Checking and Correction) memory, a fair amount of CPU power, and low power consumption. The COM Express Type 6 industry standard was chosen as it supports small and rugged form factors while providing a large array of standard interfaces. The computer chosen is the Adlink Extreme Rugged Express-IBR 3517UE with a dual-core i7 CPU and 4 GB of ECC memory. This computer does not need to be particularly synchronized, so it runs a regular Linux Ubuntu OS with minimum amount of modifications to the kernel. It can operate in air without a fan by using a heat sink, which makes it convenient to test without introducing vibrations into the system. For flight, the heat sink can be replaced by a commercially available radiating panel. The computer is rated to -40 C, although we will proceed to some tests in our chamber this year to confirm this specification.

4. POINTING LOOP TEST SETUP AND PRELIMINARY RESULTS

Maintaining good pointing accuracy is challenging in the balloon environment. The geometry and mass distribution of the whole balloon system contribute to excite pendulum motions of the gondola, which can have amplitudes up to 2 arcminutes and frequencies up to 0.5 Hz.⁹

Movements at these low frequencies are hard to reproduce on the ground, since they would require using a lifting sling just as long as the one used in flight. In addition, a simple lifting sling would not reproduce the proper torsional modes that are encountered in flight, since the payload will be attached to a long "ladder" (two slings with bars that maintain constant separation). Hence, reproducing the physical conditions for a meaningful test on the ground is a challenge.

Nevertheless, we put together a test setup to simulate some perturbations and draw some preliminary conclusions. This aims to be purely a controls system testing setup, so we can work without using the full-size BETTII truss, and work only with the exoskeleton frame shown Fig. 8. We assemble all the sensors and actuators on this structure, and hang it from an engine hoist in the high bay at NASA Goddard Space Flight Center. While hanging from the hoist, the payload can see a patch of sky, in order to use the star camera at night. Since BETTII's optics are not yet manufactured, this only tests the top-level pointing loop for the moment.

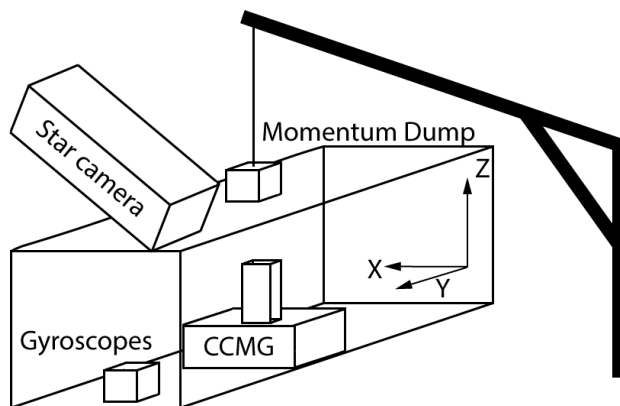


Figure 8. Sketch of the coarse loop control test setup. The setup is put in front of the doors of a high bay so that the star camera can look out on the real sky.

The payload is assembled with temporary power system, harness and controllers, and we update components one by one as they come in and pass their individual tests. When it is hanging, the system is battery powered, remote controlled, and no cables are connecting it to the ground. Presently, this test system is equipped with all flight sensors and actuators for the coarse control loop, which we are testing together and characterizing now. However, some controllers and other electronics are not yet the flight versions, but should be here during the Summer 2014.

4.1 Elevation Loop

The elevation loop is tested and tuned by putting a gyroscope onto one of our rotation stages, itself attached on the exoskeleton. The gyroscope is integrated to provide a position measurement of the rotor. In the meantime, another gyroscope is attached to the exoskeleton and measures its motion in inertial space. The control loop feeds the measured velocity of the exoskeleton to a controller that actuates the rotation stage in order to compensate for it. The gyroscope mounted on the rotation stage then tells us how close we are from canceling the motion of the exoskeleton.

Preliminary results yield a 90% rejection ratio of the pendulum perturbations, using the test rotation stage. As discussed already in Section 3.2, we anticipate significant improvements upon integrating the flight version of the rotation stages. However, the current performance is right at the limit of what is needed to maintain the guide star in the center of the field of view of the tracking channels, for the fine pointing loop.

4.2 Azimuth Loop

We test the azimuth control loop by using the CCMG, two gyroscopes, and the star camera. On this test setup, the star camera is oriented at 45 degrees from horizontal, and we suppose that 45 degrees is where we want to point. We form the cross-Elevation velocity and position estimates as a combination of the two X and Z gyroscope signals, properly rotated to account for the star camera angle. The cross-Elevation velocity and position estimates are then fed to a PID controller that commands the CCMG gimbal motor and changes the axis of rotation of the wheels to provide a torque to the whole system.

Preliminary results show our ability to cancel out the Earth's inertial motion and other perturbations down to 4" rms over periods of minutes, limited by our own actuator noise. This number is somewhat misleading, since there are no new perturbations that are injected into the system, and once it cancels out the initial perturbations and reaches steady-state, it can become more stable than the balloon environment. Also, we are limited by the noise created by the gimbal stepper motor itself, which is seen very distinctly in our gyro signal since they are attached to the same structure. We are currently investigating ways to mitigate this by changing the gear head on the stepper and using a micro-stepping scheme once our new controllers are tested.

Overall, the CCMG reaches quickly a stable control down to $< \pm 15''$ peak to valley, no matter what the initial perturbation is. Of course, for perturbations too large, the wheels' angle can get close to 90 degrees, at which point no new torque can be generated. We are currently integrating the momentum dump motor, which would relieve some of the built-up momentum into the hoist, and keep the wheels at the angle where they create maximum torque. This would allow for long-duration tests.

We have also finished integrating the star camera into the software. The image is retrieved from the camera by the flight computer, processed, and produces RA, Dec, Roll and errors which are sent to the cRIO through RS-422. Inside the cRIO, where the main control software lives, an algorithm synthesizes a variance-weighted estimate of the attitude, fusing the gyroscope information and the star camera information. The bias of the gyro is updated as well as the variance of the estimate.

While the software is functioning properly, we do not yet have results to show due to some temporary complications with the star camera which prevent us from using it. We suspect that overall stability results will not be significantly changed, except that now we have a way of confirming the stability down to the star camera accuracy ($\sim 1''$) and look at the ability to cancel out the gyroscope drift.

4.3 Status and path forward

The flight algorithm for the coarse pointing system is completed and shows good preliminary results. It allows for dynamical tuning of the PID gains of the various loops that are involved, an exercise that will have to be repeated until we reach flight configuration. In fact, we anticipate to have to tune the gains even in flight to adapt to the spectrum of perturbations that we will see. The system features a 400 Hz loop and uses about 30% of the FPGA resources of the cRIO.

The current performance of the control system on the test setup is sufficient for BETTII's coarse control loop. However, the setup of this test has much higher-bandwidth perturbations than the balloon does, due to

the geometry and stiffness of the hoist used to lift the payload. Second, the payload's inertia is very different from that of the fully-assembled BETTII. A larger inertia will allow us to make much finer azimuthal corrections within one step of the CCMG gimbal motor, while decreasing the bandwidth of the system.

There are a number of improvements scheduled to happen this year that will increase the performance of the system:

- Incorporate all flight harness into the system (July-August)
- Use new Galil controllers for all motors (July)
- Use microstepping for the Gimbal motor to smoothen the motion (July)
- Change star camera for testing purposes and convenience on the ground (August)
- Repeat pointing tests while hanging from an overhead crane instead of the small hoist (August)
- Assemble exoskeleton and truss into final flight configuration, to recreate the correct inertia (Fall)
- Integrate with the fine pointing loop and the tip/tilt mirrors (Fall, need BETTII optics and dewar)

By the end of the year, a complete characterization of the coarse control system will be achieved on BETTII in a flight-like configuration. Also, we will start incorporating the tip/tilt mirrors and H1RG angle sensor once the optics and dewar are available.

5. CONCLUSION

The architecture of BETTII's control system has three nested levels of control, organized around an alt/az pointing system with fast-steering tip/tilt mirrors for fine pointing. The fine pointing control relies on finding a guide star on the angle sensor. The phase control depends on our ability to properly estimate the attitude and correct phase offsets on a regular basis with a phase calibrator. The various loops are synchronized by one master heart beat at ~ 400 Hz. All of the hardware for the control system has been acquired and most has successfully passed environmental testing. A first-level pointing setup shows good performance of the actuators and sensors, and promises excellent flight pointing control and knowledge capabilities once the full system is integrated.

REFERENCES

- [1] Rinehart, S., "The Balloon Experimental Twin Telescope for Infrared Interferometry (BETTII)," *Optical and Infrared Interferometry II. Edited by Danchi* **7734**, 16 (July 2010).
- [2] Mariotti, J.-M. and Ridgway, S. T., "Double Fourier spatio-spectral interferometry - Combining high spectral and high spatial resolution in the near infrared," *Astronomy and Astrophysics (ISSN 0004-6361)* **195**, 350 (Apr. 1988).
- [3] Leisawitz, D., Bolcar, M. R., Lyon, R. G., Maher, S. F., Memarsadeghi, N., Rinehart, S. A., and Sinukoff, E. J., "Developing wide-field spatio-spectral interferometry for far-infrared space applications," in [*Optical and Infrared Interferometry III. Proceedings of the SPIE*], NASA Goddard Space Flight Ctr. (United States) (July 2012).
- [4] Ohta, I. S., Hattori, M., and Matsuo, H., "Development of a multi-Fourier-transform interferometer: fundamentals," *Applied Optics IP* **45**, 2576-2585 (Apr. 2006).
- [5] Helmich, F. P. and Ivison, R. J., "FIRI—A far-infrared interferometer," *Experimental Astronomy* **23**, 245-276 (Mar. 2009).

- [6] Leisawitz, D., Baker, C., Barger, A., Benford, D., Blain, A., Boyle, R., Broderick, R., Budinoff, J., Carpenter, J., Caverly, R., Chen, P., Cooley, S., Cottingham, C., Crooke, J., Dipietro, D., Dipirro, M., Femiano, M., Ferrer, A., Fischer, J., Gardner, J. P., Hallock, L., Harris, K., Hartman, K., Harwit, M., Hillenbrand, L., Hyde, T., Jones, D., Kellogg, J., Kogut, A., Kuchner, M., Lawson, B., Lecha, J., Lecha, M., Mainzer, A., Mannion, J., Martino, A., Mason, P., Mather, J., McDonald, G., Mills, R., Mundy, L., Ollendorf, S., Pellicciotti, J., Quinn, D., Rhee, K., Rinehart, S., Sauerwine, T., Silverberg, R., Smith, T., Stacey, G., Stahl, H. P., Staguhn, J., Tompkins, S., Tveekrem, J., Wall, S., and Wilson, M., "The space infrared interferometric telescope (SPIRIT): High-resolution imaging and spectroscopy in the far-infrared," *Advances in Space Research* **40**, 689 (Jan. 2007).
- [7] Harwit, M., Leisawitz, D., and Rinehart, S., "A far-infrared/submillimeter kilometer-baseline interferometer in space," *New Astronomy Reviews* **50**, 228 (Mar. 2006).
- [8] Davis, S. P., Abrams, M. C., and Brault, J. W., "Fourier transform spectrometry," *Fourier transform spectrometry by Sumner P. Davis et al. San Diego* (Jan. 2001).
- [9] Fixsen, D. J., Cheng, E. S., Cottingham, D. A., Folz, W. C., Inman, C. A., Kowitt, M. S., Meyer, S. S., Page, L. A., Puchalla, J. L., Ruhl, J. E., and Silverberg, R. F., "A Balloon-borne Millimeter-Wave Telescope for Cosmic Microwave Background Anisotropy Measurements," *Astrophysical Journal v.470* **470**, 63 (Oct. 1996).
- [10] Fixsen, D. J., Cheng, E. S., Cottingham, D. A., Eplee, R. E., Hewagama, T., Isaacman, R. B., Jensen, K. A., Mather, J. C., Massa, D. L., Meyer, S. S., Noerdlinger, P. D., Read, S. M., Rosen, L. P., Shafer, R. A., Trenholme, A. R., Weiss, R., Bennett, C. L., Boggess, N. W., Wilkinson, D. T., and Wright, E. L., "Calibration of the COBE FIRAS instrument," *The Astrophysical Journal* **420**, 457 (Jan. 1994).
- [11] Mendillo, C. B., Chakrabarti, S., Cook, T. A., Hicks, B. A., and Lane, B. F., "Flight demonstration of a milliarcsecond pointing system for direct exoplanet imaging," *Applied Optics* **51**, 7069 (Oct. 2012).
- [12] Oxley, P., Ade, P. A., Baccigalupi, C., deBernardis, P., Cho, H.-M., Devlin, M. J., Hanany, S., Johnson, B. R., Jones, T., Lee, A. T., Matsumura, T., Miller, A. D., Milligan, M., Renbarger, T., Spieler, H. G., Stompor, R., Tucker, G. S., and Zaldarriaga, M., "The EBEX experiment," *Infrared Spaceborne Remote Sensing XII. Edited by Strojnik* **5543**, 320–331 (Nov. 2004).